Analyzing Environmental Effects on the Mechanical Performance of Composite Reinforcement Systems

Haji Akbar Sultani(✉), Arvydas Rimkus, Aleksandr Sokolov, and Viktor Gribniak

Vilnius Gediminas Technical University, Sauletekio Av. 11, Vilnius, LT 10223, Lithuania
haji-akbar.sultani@vilniustech.lt

Abstract. In recent years, fiber-reinforced polymeric (FRP) materials have become promising alternatives to steel because of their lightweight, electromagnetic transparency, and corrosion resistance. However, the unfavorable environment (elevated temperature and high humidity in particular) can affect the long-term mechanical performance of these materials. Therefore, this study utilizes the previously developed testing layout and analytical model to simulate and quantify these unfavorable effects in concrete beams reinforced with FRP composites. The explicit analytical model quantifies the flexural stiffness reduction expressed in the equivalent stresses acting on the tensile concrete. This approach does not require specifying the loading history that makes it feasible for the comparative analysis of the stiffness degradation of FRP-reinforced concrete via a series of repeated mechanical tests corresponding to continuous exposition to the harsh environment. This study considers the open atmosphere corresponding to the Nord Europe climatic region. In addition, after applying the service load, the reference specimens were kept under laboratory conditions. The latter samples provide the reference for quantifying the stiffness degradation and the repeated mechanical load effect expressed in the residual deflection of the test sample. Thus, this study reveals that the open environment specifically affected the stiffness decay in the external bonded reinforcement system. In contrast, this effect in the near-surface mounted reinforcement system was insignificant.

Keywords: Reinforced Concrete · FRP Composites · Residual Stiffness · Analytical Model · Flexural Test

1 Introduction

Current reinforcement technologies provide various materials for strengthening concrete structures (Gribniak[1]). Fiber-reinforced polymers (FRP) are a promising alternative to steel reinforcement due to their high strength, lightweight, corrosion resistance, and electromagnetic transparency (Jakubovskis[2]). However, the relatively low resistance to ultraviolet radiation, high humidity, and high temperature may degrade the mechanical characteristics of FRP materials over time (Liu[3]), (Bazli[4]). In addition, different types of FRP reinforcement systems, i.e., near-surface mounted (NSM) strips and

A. Ilki et al. (Eds.): *fib* Symposium 2023, LNCE 349, pp. 618–627, 2023.
https://doi.org/10.1007/978-3-031-32519-9_60

externally bonded reinforcement (EBR) sheets, exhibit diverse effects on the mechanical properties of composite systems (Gribniak[5]). This study aims to apply a recently developed test setup and simplified analytical model (Gribniak[6])to analyze the residual bending stiffness of standardized laboratory specimens. The study uses an equivalent residual stiffness method to measure the structural performance of composite reinforcement systems exposed to open environment conditions. This study considers the open a corresponding to the Nord Europe climatic region. The applied analytical model explicitly relates the specific moments and curvature values, quantifying the equivalent stresses acting in the concrete belonging to the tension zone. The model assumes the rectangular distribution of the stresses in the tensile concrete. On the one hand, such a simplification allows an acceptable approximation of the tension stiffening stresses (Gribniak[6]). On the other hand, the residual stress quantification (inverse analysis) does not require iterative calculations, which makes it suitable for the current research purposes.

This manuscript presents partial results of an ongoing test program using 34 test specimens with different layouts and combinations of composite reinforcement; this manuscript presents partial results for 10 samples to illustrate the proposed analysis procedure. First, the specimens were subjected to service loads. Then, the reference samples were stored under laboratory conditions; alternative elements exposed to open air outside the building evaluated environmental effects on stiffness degradation.

2 Beam Tests

The previous studies (Gribniak[5]), (Gribniak[6])established the geometry and the testing layout of the bending specimens—following the formation of multiple cracks in a relatively small laboratory sample, thus reducing the discrete cracking effect on the curvature estimation result. In addition, the cross-section of the beam specimens was designed to satisfy the simplified modeling assumption (i.e., rectangular tension stress distribution in the concrete). Thus, the corresponding "exact" tension-stiffening diagram (Gribniak et al.[7]) had a rectangular shape similar to the simplified one. Remarkably, the proposed analytical model does not define a specific constitutional law: the equivalent stresses only evaluate the residual flexural stiffness to analyze the long-term deterioration of the mechanical properties of the composite reinforcement.

This study considers the 1000 mm long slab-shaped beams loaded in the four-point schemes, as Figs. 1 and 2 show. The 200 × 100 mm cross-section was reinforced with near-surface mounted (NSM) strips, embedded bars, and externally bonded reinforcement (EBR) sheets in various combinations. This study includes ten specimens and two reinforcement types, i.e., CFRP EBR sheets and NSM strips adhesively attached to the most tensioned surface of the beam samples. Table 1 specifies the characteristics of the test specimens. In this table, h and b denote the cross-section height and width; d stands for the effective depth of the reinforcement layer; A_r and E_r indicate the reinforcement area and modulus of elasticity; f_{cm} is the compressive strength of the Ø150 × 300 mm concrete cylinder at the age of 87 days; t describes the specimens' age corresponding to the first and second testing stages.

The beam specimens were produced using laboratory-mixed concrete. The mix proportions for one cubic meter are following: the cement CEM I 42.5 R = 356 kg, water =

163 l, the limestone powder = 177 kg, the 0/4 mm sand = 890 kg, the 4/16 mm crushed dolomite aggregates = 801 kg, the superplasticizer Mapei Dynamon XTend = 1.97% (by the cement weight), and the admixture SCP 1000 Optimiser = 3.5 kg. The mixture also encompassed 0.9 kg Crackstop M Ultra synthetic micro-fibers and 4.2 kg Durus EasyFinish synthetic macro-fibers.

Two unidirectional MapeWrap C UNI-AX sheets with the dry fabric's 100 × 0.164 mm equivalent thickness were used in the EBR reinforcement system. The manufacturer reported the CFRP material's 4830 MPa tensile strength and 230 GPa modulus of elasticity. Before the EBR bonding, the cleaned concrete surface was leveled with epoxy putty and primer. Then, the wet lay-up system employed the two-component epoxy resin MapeWrap 31 to fix the CFRP sheets. The NSM reinforcement system was composed of a pultruded 10 × 1.4 mm carbon FRP strip (S&P C-Laminate); the strips were installed in the 4 × 12 mm grooves. The two-component epoxy adhesive S&P Resin 220 filled these grooves before the strip installation. The EBR and NSM systems were installed seven days before the mechanical tests to form a reliable adhesion contact between FRP materials and concrete.

The specimens were subjected to monotonically increasing and repeating loads using a 5 MN capacity servo-hydraulic testing machine under displacement control and the 0.4 mm/min loading speed: two sets of linear variable displacement transducers (LVDT) capture the vertical and longitudinal displacements, and a digital image correlation (DIC) system monitors the cracking process and surface deformations; the LVDT and DIC system capture deformations of the opposite sides denoted as "①" and "②" in Fig. 2. Thus, the LVDT devices L_{10}–L_{15} estimate deformations of the side surface ①, and L_1–L_3, L_4–L_6, and L_7–L_9 indicators monitor the vertical displacements. The data logger ALMEMO 5690–2 collects the load cell and LVDT outputs every second.

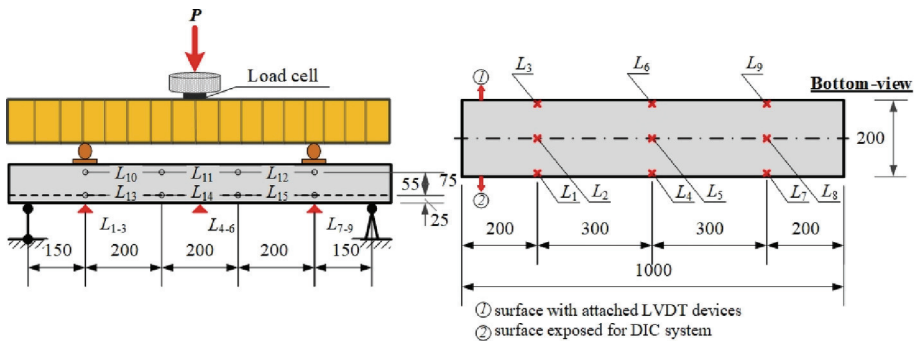

Fig. 1. The loading scheme and indicators' distribution.

The test samples were subjected to repeated loads to investigate the stiffness decay. The beams were subjected to five load cycles fluctuating around the service moment, nominally representing 55% of the ultimate load. The previous studies (Gribniak[5]), (Gribniak[6]) identified the load-bearing capacity of the beam samples, which was almost identical for the EBR and NSM reinforcement systems. Therefore, these tests

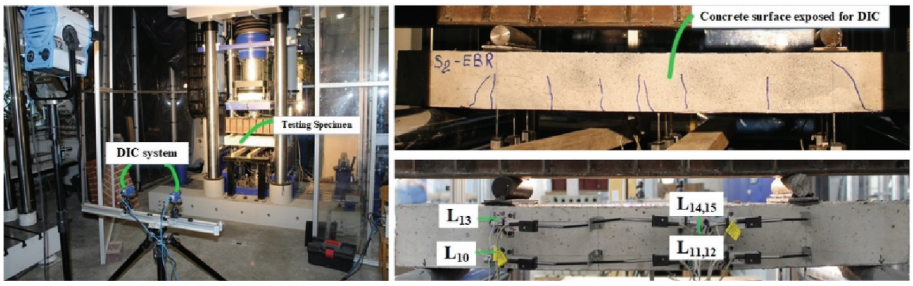

Fig. 2. The experimental testing setup.

assume identical the 3.710 kN service moments for all considered beams (Table1) and correspondingly 3.075 kN and 4.125 kN boundary moments for the load cycles.

Table 1. Main parameters of the beam samples and material properties of the analyzed beams.

Beam	h [mm]	b [mm]	d [mm]	A_r [mm^2]	E_r [GPa]	$n\rho$ [%]	f_{cm} [MPa]	t [days]
B1-NSM*	103	199	93	28.0	170	0.73	48.14	120/274
B2-NSM*	104	198	94	28.0	170	0.73	48.14	119/274
B3-EBR*	104	198	105	32.8	230	0.73	48.14	119/274
B4-EBR*	105	197	106	32.8	230	0.68	60.5	116/271
B5-EBR**	105	201	105	32.8	230	0.71	48.14	120/274
B6-EBR**	104	198	105	32.8	230	0.72	48.14	119/276
B7-EBR**	106	197	107	32.8	230	0.72	48.14	119/273
B8-NSM**	103	200	93	28.0	170	0.68	60.5	116/273
B9-NSM**	102	200	92	28.0	170	0.69	60.5	117/270
B10-NSM**	100	201	90	28.0	170	0.70	60.5	116/270

(*) Specimen stored in laboratory conditions.
(**) Sample exposed to the open air outside the laboratory.

3 Analytical Model

The study (Gribniak[6]) proved the suitability of the simplified analytical model. Thus, this manuscript provides only the explanations necessary to identify the regression trends estimating the environmental effects on the residual stiffness of the beam specimens. Figure3 shows a schematic of the model, which uses the following simplifications:

- The Euler-Bernoulli hypothesis is valid. The interested reader can find the justification of this assumption for reinforced concrete beams elsewhere (e.g., (Dulinskas et al.[8]), (Gribniak[9])).

- The concrete cracking process follows a smeared crack pattern. Numerous literature examples (e.g., (Gribniak et al.[7]), (Gribniak[9])) proved the adequacy of this assumption.
- Perfect elastic deformation models describe the behavior of all reinforcement materials and compressive concrete. This assumption simplifies the analytical expressions.
- Tensile stresses in concrete are distributed rectangularly, determining the equivalent stress value. This fundamental simplification allows for avoiding iterative calculations. Thus, it becomes possible to quantify the residual stiffness of repeatedly loaded composite elements.

Figures 3b and 3c demonstrate the strain and strain distribution in the transformed section. The rectangular stress approximation defines the equivalent stress value (Fig. 3d), which is the further analysis object.

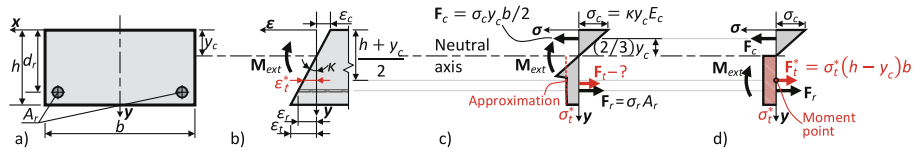

Fig. 3. Analytical model of the pure bending zone (Gribniak[6]): a) transformed cross-section; b) strain distribution; c) stress distribution; d) the equivalent stress approach.

The equilibrium equations of internal forces and bending moments for the centroid of the equivalent tensile stress diagram (Fig. 3d) govern the residual stiffness model:

$$\mathbf{F}_t^* + \mathbf{F}_r - \mathbf{F}_c = 0;\ \mathbf{F}_r\left(d_r - \tfrac{h+y_c}{2}\right) + \mathbf{F}_c\left(\tfrac{h+y_c}{2} - \tfrac{y_c}{3}\right) - \mathbf{M}_{ext} = 0, \tag{1}$$

where $\mathbf{F}_t^*$ is the equivalent resultant force in the tensile concrete; $\mathbf{F}_r$ and $\mathbf{F}_c$ are the internal forces acting on the tensile reinforcement and the compressive concrete; Fig. 3 describes the remaining notations. The above equation system relates the internal forces and stresses (Figs. 3c and 3d), employing the strain compatibility condition (Fig. 3b). An interested reader can find further explanations in the article (Gribniak[6]). The resulting equation defines the third-order polynomial of the neutral axis ordinatey_c:

$$C_3 y_c^3 + C_2 y_c^2 + C_1 y_c + C_0 = 0 \tag{2}$$

with coefficients

$$C_3 = \tfrac{E_c b}{6E_r A_r},\ C_2 = 1 + \tfrac{E_c bh}{2E_r A_r},\ C_1 = h - 3d_r,\ C_0 = 2d_r^2 - hd_r - \tfrac{2\mathbf{M}_{ext}}{\kappa E_r A_r}. \tag{3}$$

The above polynomial has 3 roots, and the condition 0 < yc ≤ h defines the ordinate:

$$y_c = \frac{1}{3C_3}\left\{2\sqrt{C_2^2 - 3C_3C_1}\cos\left(\frac{1}{3}\cos^{-1}\left\{-\frac{27C_3^2C_0 - 9C_3C_2C_1 + 2C_2^3}{2\sqrt{\left[C_2^2 - 3C_3C_1\right]^3}}\right\}\right) - C_2\right\}. \tag{4}$$

The equivalent stress (Fig. 3d) and strain (Fig. 3b) can be found as follows:

$$\sigma_t^* = \kappa \frac{y_c^2 bE_c - 2(d_r - y_c)E_r A_r}{2(h - y_c)b},\ \varepsilon_t^* = \kappa \frac{h - y_c}{2}. \tag{5}$$

4 Test Results and Discussion

This study considers the mechanical performance of the pure bending zone. The indicator distribution scheme (Figs. 1 and 2) ensures the curvature estimation using three independent measurement sets, i.e., the vertical displacement registered by L_1-L_9 LVDT devices and the surface deformation captured by the DIC and L_{10}-L_{15} LVDT. Thus, the beam specimens underwent two stages of testing under repeated load. After the first loading stage, the reference samples were stored under laboratory conditions; alternate samples were exposed to open air outside the laboratory building. For instance, identical reference specimens (B1–B4 in Table 1) were stored in the laboratory, while the remaining six alternative samples were exposed to an open environment. Figure 4 describes the environmental conditions; the laboratory specimens were kept at an average relative humidity of 35% and 20.5 °C. The tests were repeated after half a year.

The following analysis uses the vertical displacement monitoring results for determining the equivalent stress (Eq. 4). The following equation defines the curvature values necessary for the analysis:

$$\kappa = \frac{8 \cdot \delta}{l_b^2 + 4 \cdot \delta^2},\ \delta = \frac{\delta_4 + \delta_5 + \delta_6}{3} - \frac{\delta_1 + \delta_2 + \delta_3 + \delta_7 + \delta_8 + \delta_9}{6}, \tag{5}$$

where δ is the deflection over the pure bending zone; δ_i is the displacement obtained by LVDT L_i ($i = 1 \ldots 9$, Fig. 1); l_b ($= 600$ mm) is the pure bending zone length.

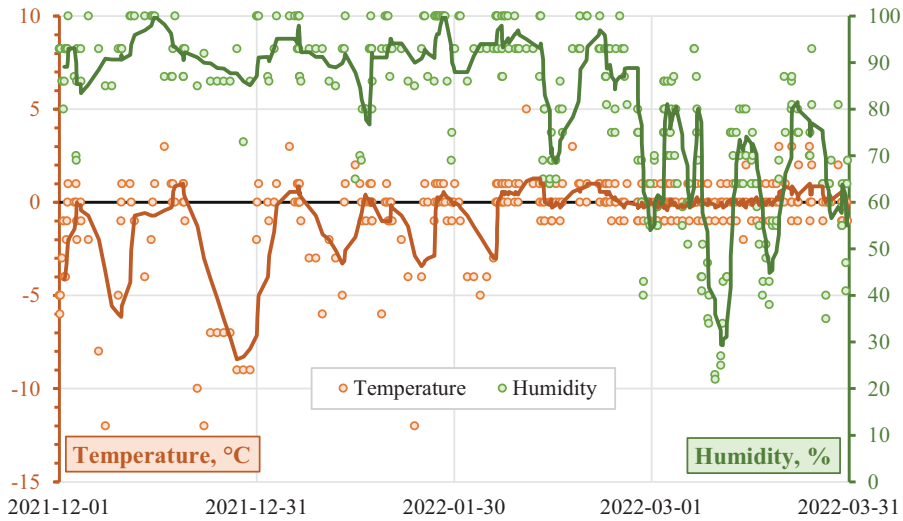

Fig. 4. Environmental conditions outside the laboratory building.

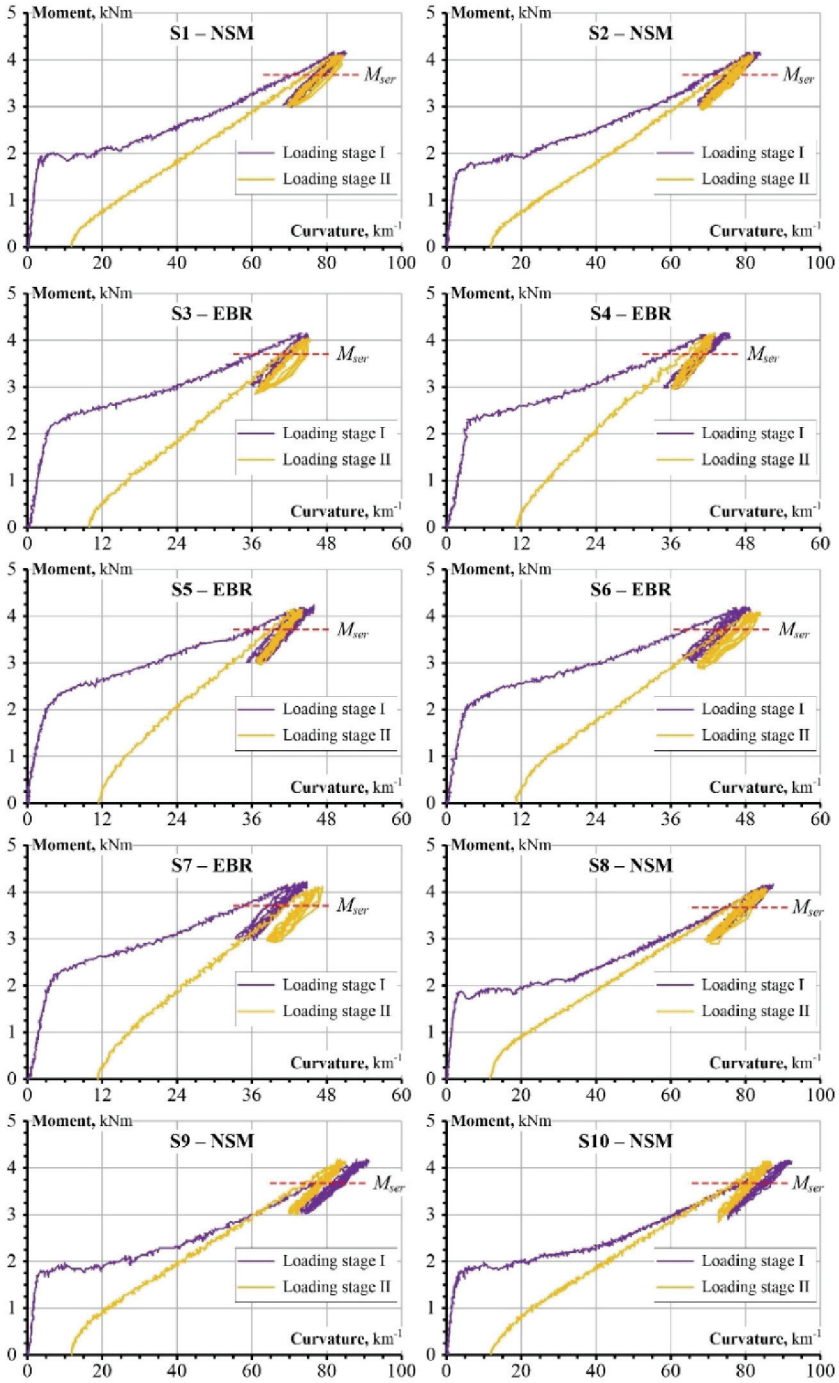

Fig. 5. The moment-curvature results of the test samples from Table 1.

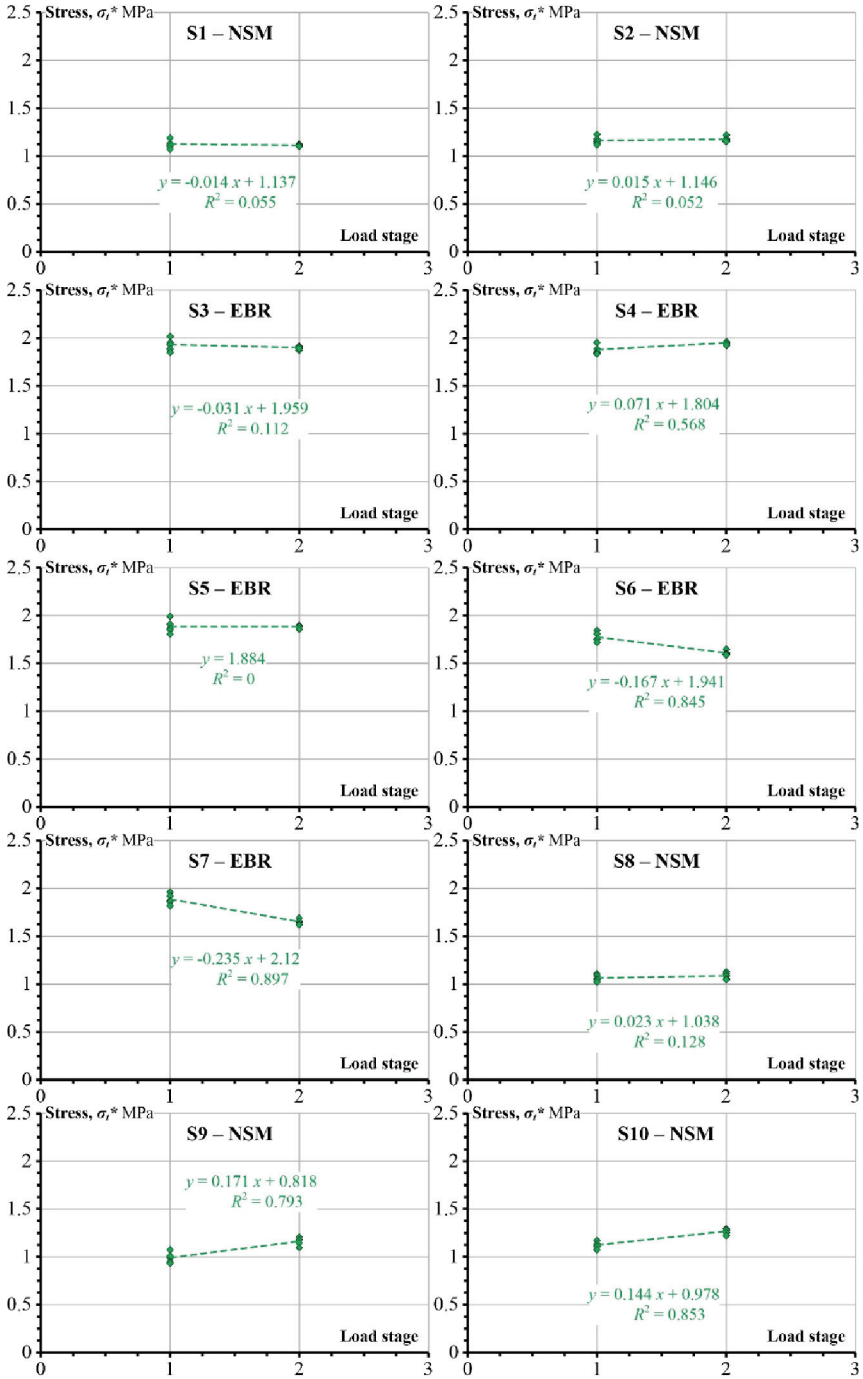

Fig. 6. Equivalent tensile stress (σ_t^*) corresponding to two loading stages.

Figure 5 shows the moment-curvature diagrams of the beam specimens from Table 1. The black lines correspond to the results of the first loading stage; the green lines describe the results of the beams during the second loading stage (after exposure of the samples in an open environment or laboratory conditions). The loop branch of the diagram corresponds to the repeated loading.

Remarkably, the equivalent stress σ_t^* calculations (Sect. 3) do not require loading history knowledge—the analysis only needs a particular moment and curve values to calculate the equivalent stress. In this study, the service moment (red line in Fig. 5) defines the target load. Thus, the stiffness decay analysis employs the curvature values of the ascending diagram branch in Fig. 5. Therefore, each test generated five load points; the first load was skipped to avoid regression skewness due to the excessive stiffness of the beam experiencing the first load.

Figure 6 shows the equivalent stresses corresponding to these two loading stages. The regression lines highlight the decreasing trend in stiffness. As noted (Table 1), the S1–S4 samples are the reference beams stored in the laboratory. None of those elements reveals stiffness decay during the second load stage (Fig. 6). On the contrary, the EBR systems were susceptible to the environmental conditions—an average of 16% decay in the equivalent stresses was observed after exposing the beams in the open environment. The slope coefficient quantifies the decay. At the same time, the NSM samples were more resistant to the open environment conditions than the EBR beams were.

However, the limited number of test specimens and the duration of the environmental effects do not allow for the formulation of definitive conclusions. Remarkably, the reported results provide a first attempt at identifying the stiffness decay in composite reinforcement systems, representing a part of the ongoing research project. Further tests will verify the hypothesized vulnerability of the EBR systems to environmental conditions, though the proposed testing setup demonstrated its capability to estimate the stiffness decay.

5 Concluding Remark

This paper presents a new test setup and analysis methodology for the long-term degradation analysis of concrete beams with composite reinforcement systems. The manuscript presents the partial results of an ongoing test program. This illustrative study includes ten selected beam specimens subjected to four-point bending. The tests revealed a particular vulnerability of the externally bonded reinforcement (EBR) systems to environmental conditions. The near-surface mounted (NSM) reinforcement systems were less susceptible to the storing conditions. Remarkably, the reported results define a first attempt at identifying the stiffness decay in composite reinforcement systems, representing a part of the ongoing research project. However, the proposed testing setup demonstrated its capability to estimate the stiffness decay. Further tests will check the hypothesized peculiarity of the EBR systems.

Acknowledgment. The authors acknowledged financial support from the European Regional Development Fund (Project No 01.2.2-LMT-K-718–03-0010) under a grant agreement with the Research Council of Lithuania (LMTLT).

References

1. Gribniak V (2020) Special issue advanced composites: from materials characterization to structural application. Materials 13(24) Paper ID: 5820. doi:https://doi.org/10.3390/ma13245820
2. Jakubovskis R, Gintaris K, Viktor G, André W, Mantas J (2014) Serviceability analysis of concrete beams with different arrangements of GFRP bars in the tensile zone. ASCE Journal of Composites for Construction 18(5) Paper ID: 04014005. doi: https://doi.org/10.1061/(ASCE)CC.1943-5614.0000465
3. Liu T, Xing L, Peng F (2020) A comprehensive review on mechanical properties of pultruded FRP composites subjected to long-term environmental effects. Compos Part B: Eng 191 Paper ID: 107958. doi:https://doi.org/10.1016/j.compositesb.2020.107958
4. Bazli M, Armin J, Hamed A, Zhao X-L, Yu B, Singh Raman RK (2020) Effects of UV radiation, moisture and elevated temperature on mechanical properties of GFRP pultruded profiles. Construct Build Mater 231 Paper ID: 117137. doi:https://doi.org/10.1016/j.conbuildmat.2019.117137
5. Gribniak V, Aleksandr S, Arvydas R, Sultani HA, Tuncay MC, Torres L (2019) A novel approach to residual stiffness of flexural concrete elements with composite reinforcement. In: Article in Proceedings of the IABSE Symposium – Towards a Resilient Built Environment Risk and Asset Management, 27–29 March 2019, Guimarães, Portugal. Zurich: IABSE, 46–51
6. Gribniak, V, Sultani HA, Rimkus A, Sokolov A, Torres L (2021) Standardised quantification of structural efficiency of hybrid reinforcement systems for developing concrete composites. Compos Struct 274 Paper ID: 114357. doi:https://doi.org/10.1016/j.compstruct.2021.114357
7. Gribniak V, Kaklauskas G, Juozapaitis A, Kliukas R, Meskenas A (2017) Efficient technique for constitutive analysis of reinforced concrete flexural members. Inverse Problems in Science and Engineering 25(1):27–40. https://doi.org/10.1080/17415977.2015.1135139
8. Dulinskas E, Gribniak V, Kaklauskas G (2008) Influence of steam curing on high-cyclic behaviour of prestressed concrete bridge elements. The Baltic Journal of Road and Bridge Engineering 3(3):115–120. https://doi.org/10.3846/1822-427X.2008.3.115-120
9. Gribniak V, Kaklauskas G, Bacinskas D (2009) Experimental investigation of shrinkage influence on tension stiffening of rc beams In: Article in Proceedings of the Eighth International Conference: Creep, Shrinkage and Durability of Concrete and Concrete Structures (ConCreep 8), vol 1, pp 571–577, Ise-Shima, Japan, 2008. London: CRC Press/Balkema, Taylor & Francis Group
10. Sultani HA, Rimkus A, Sokolov A, Gribniak V (2022) A new testing procedure to quantify unfavourable environmental effect on mechanical performance of composite reinforcement system. In: Proceedings of the 14th fib International Ph.D. Symposium in Civil Engineering, 5–7 September 2022, Rome, Italy. Lausanne: fib, pp 377–384